Simulations of Local Oxidation Nanolithography by AFM Based on the Generated Electric Field

L. Filipovic*† and S. Selberherr*
*Institute for Microelectronics, TU Wien, Gußhausstraße 27–29/E360, A-1040 Wien, Austria
†Christian Doppler Laboratory for Reliability Issues in Microelectronics
Email: filipovic|selberherr@iue.tuwien.ac.at

***Abstract*—During the last decades it has become evident that novel lithographic techniques are required in order to fabricate nanosized devices. It has been shown that non-contact AFM is an efficient technique, capable of manufacturing nanometer sized devices on the surface of a silicon wafer. The AFM nanooxidation approach is based on generating a potential difference between a cantilever needle tip and a silicon wafer. A simulator for nanooxidation with non-contact AFM tools was developed. The presented model uses empirical equations for the height and half-width of an AFM nanodot with a physics based shape model. The shape model uses a particle distribution directly derived from the surface charge density, generated on the silicon surface due to the strong electric field in the region.**

I. Introduction

Conventional photolithographic methods, which are derived from optical and electron beam lithographies, are no longer capable of providing the necessary processing steps for the fabrication of modern nanosized devices. They are either too cost intensive or unsuitable for handling the extensive variety of organic and biological systems applicable to nanotechnology [1]. Likewise, conventional simulators, which deal with topographical changes to silicon wafers due to the application of physical or chemical processing steps, can no longer model the processes required for the generation of nanoscale structures. During the last decades, alternatives to conventional photolithography were actively investigated, such as nanoimprint lithography [2], soft lithography [3], and scanning probe lithography [4]. The most promising method for nanofabrication was found to be scanning probe oxidation, or Local Oxidation Nanolithography (LON). The reasons behind the success of LON are bountiful, among the most important being its ability to be performed at room temperature and across a large range of materials.

A. Local Oxidation Nanolithograpy

The development of LON originated with the development of the scanning probe microscope in the 1980s [5], followed by the atomic force microscope (AFM) in 1986 [6], as tools to utilize tunneling current and/or electrostatic forces between a conductive cantilever tip and a sample surface in order to detect and measure depressions and protuberances on a nanometer sized section of a sample surface. AFM has been used extensively, not only in the semiconductor industry, but also in physics, chemistry, biology, biochemistry, and other disciplines, where the chemical or physical properties of a surface are required [7]. Local anodic oxidation of semiconductor surfaces was suggested by Dagata et al. [4] as a method to modify semiconductor surfaces with nanoscale precision. More recently LON has been studied and improved for use as a patterning tool for the deposition, removal, and modification of material surfaces with nanoscale precision [8], [9], [10]. After the initial work with a STM microscope, similar processes have been reported using an AFM microscope with a conductive probe attached to a cantilever in contact and non-contact modes [9], [10]. A distinct advantage of AFM over STM is its ability to read back the actual topography of the generated pattern, while STM is unable to show the real height. In addition, the advantage of noncontact mode AFM over contact mode AFM is the increased reliability of the AFM needle tip [11]. Contact mode AFM causes the needle tip to degrade much faster due to the repeated contact with the semiconductor surface during operation. The models presented here deal with LON patterns generated with an AFM device operating in noncontact mode, as this was found to be the most promising method for generating narrow patterns at relatively high speeds.

II. Modeling of nc-AFM Nanodots and Nanowires

As shown in Fig. 1, the first step of nanopatterning with AFM is the application of a voltage bias to the tip of an AFM needle and bringing the needle in close proximity to a substrate surface. Due to the high electric field generated in the region and the relative humidity of the ambient, a water meniscus (or water bridge) is formed, providing an electrolyte between the needle (cathode) and the sample surface (anode). The presence of the water meniscus limits the lateral diffusion of anions, thereby limiting the lateral extensions of the AFM nanodot. Inside the water meniscus, oxyanions (OH-) are generated due to the high electric field. The oxyanions then undergo an oxidation reaction through interaction with the silicon surface. For a silicon wafer, the oxidation reaction, including holes (h+) and electrons (e-), at the anode end (silicon surface) is

$$Si + 2h^+ + 2\left(OH^-\right) \rightarrow Si\left(OH\right)_2 \rightarrow SiO_2 + 2H^+ + 2e^-, \quad (1)$$

while the reaction at the cathode end (AFM needle tip), from [1] is

$$2H^+_{(aq)} + 2e^- \rightarrow H_2. \quad (2)$$

ISBN 978-0-615-71756-2

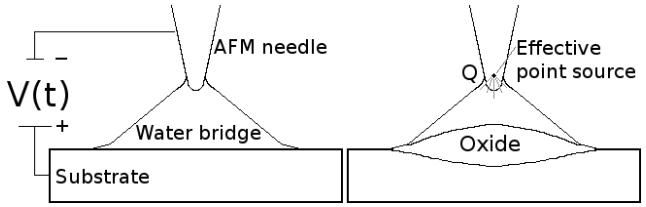

Fig. 1. Basic schematic for LON with an AFM needle and the simulation model, which treats the AFM needle as a point charge.

There is a variety of factors which affect the geometry of a generated nanodot, such as pulse time, applied bias voltage, relative humidity, and tip shape. Three types of AFM tip shapes have been analyzed in the literature [12]. The different shapes are for a rough, hemispherical, and blunt tip configuration, which can be modeled using a ring charge, point charge, and line charge, respectively. We present two models: one for a hemispherical tip shape, which involves only one charged dot and one for all other tip shapes, where multiple charged dots are required in order to model the needle tip. For the implemented model, it is assumed that all oxyanions are generated at the effective point source of the AFM needle tip. This simplifies the model, while not having a significant consequence on the model's accuracy [13]. The oxyanions traverse through the water meniscus along electric field lines, finally colliding with the sample surface, whose evolution is modeled using the Level Set method [14].

Neglecting the effects of surrounding ions on the electric field strength and recombination reactions between ions to form water, the voltage and electric field strength in the water meniscus region can be calculated using the image charge method [12], [13], [15]. Mesa et al. [15] suggest that each AFM needle can be represented as a series of charged particles distributed along the structure of the needle. The presented model implements this idea with the use of point charges, which is valid for all types of AFM needles. The electric field is then calculated and the Surface Charge Density (SCD) distribution along the substrate surface is found. The oxyanion distribution along the silicon surface drives the oxidation reaction; therefore, the shape of an AFM generated nanodot follows the SCD distribution.

A. SCD Distribution for a Hemispherical Needle Tip

As discussed in the previous section, the model representing the shape of a hemispherical AFM generated nanodot follows the SCD distribution, which is derived by replacing the AFM needle tip with an effective point source Q and the silicon substrate surface by an infinitely long conducting plane. The image charge method is then applied to find the voltage at every location in the water meniscus region p(x,y,z):

$$V\left(\vec{p}\right) = k\left[\frac{Q}{\left(x^2+y^2+(z-D)^2\right)^{1/2}} - \frac{Q}{\left(x^2+y^2+(z+D)^2\right)^{1/2}}\right], \tag{3}$$

where $k = 1/4\pi\epsilon_r\epsilon_0$, Q is the effective point charge at a distance D from the surface, and ϵ_r is the relative permittivity of water. Given $\vec{E} = -\vec{\nabla}V$ the electric field strength can be found:

$$E_z = kQ\left[\frac{z-D}{\left(x^2+y^2+(z-D)^2\right)^{3/2}} - \frac{z-D}{\left(x^2+y^2+(z+D)^2\right)^{3/2}}\right]. \tag{4}$$

The induced SCD on the surface is represented as $\sigma\left(x,y,0\right) = \epsilon_r\epsilon_0 E_z\left(x,y,0\right)$, leading to the expression

$$\sigma\left(x,y,0\right) = \frac{-DQ}{2\pi\left(x^2+y^2+D^2\right)^{3/2}}. \tag{5}$$

A model has already been developed which utilizes (5) in order to generate a topographical representation of an AFM nanodot [16]. However, the model implements a Monte Carlo rejection technique to build the nanodot, which is very time and memory expensive, when large aspect ratio problems are required.

B. SCD Distribution for a Routh Needle Tip

As mentioned in [12], in order to simulate the nanodot growth, initiated using a rough AFM tip, the needle may be modeled as a ring of charges at a given height above the silicon surface. The ring of charges is modeled by a desired number of dot charges surrounding the AFM tip cirumference. When multiple dot charges are used to represent the AFM needle, the equation for the surface charge density becomes

$$\sigma\left(x,y,0\right) = -\frac{D}{2\pi}\sum_{i=1}^{N}\frac{Q_i}{\left[\left(x-x_i\right)^2+\left(y-y_i\right)^2+D^2\right]^{3/2}}, \tag{6}$$

where N is the total number of charged dots, Q_i and (x_i, y_i, D) are the effective charge and the location of the i^{th} dot, respectively. The maximum possible SCD distribution occurs, when all the charges are concentrated at a single point, making the charged circle's radius zero:

$$\sigma_{max} = N\frac{Q_{tot}}{2\pi D^2}. \tag{7}$$

III. SCD Based Particle Distribution Modeling

A. One-Dimensional SCD Distribution

When performing AFM nanodot simulations for a two-dimensional model, a one-dimensional particle distribution is required. (5) can be re-written in a one-dimensional form:

$$\sigma\left(x,0\right) = \frac{-DQ}{2\pi\left(x^2+D^2\right)^{3/2}}. \tag{8}$$

(8) is used in order to generate a one-dimensional Probability Density Function (PDF)

$$f\left(x\right) = -C\frac{DQ}{2\pi\left(x^2+D^2\right)^{3/2}}, \tag{9}$$

where C is the normalization constant. C is found by integrating $f\left(x\right)$ over the entire simulation domain and equating it to unity:

$$\int_{-\infty}^{\infty} f\left(x\right)dx = -C\int_{-\infty}^{\infty}\frac{DQ}{2\pi\left(x^2+D^2\right)^{3/2}}dx = 1. \tag{10}$$

Solving (10), we find that $C = -\pi D/Q$, which is then substituted into (9) to form the normalized PDF for a one-dimensional SCD distribution

$$f(x) = \frac{D^2}{2\left(x^2 + D^2\right)^{3/2}}. \tag{11}$$

The next step is finding the Cumulative Probability Distribution (CPD) function, derived by integrating the normalized PDF, $\Phi(r) = \int_{-\infty}^{r} f(x)dx$, where r is the SCD distributed radius. Because of the symmetry of the SCD distribution on either side of the charged particle Q, generating a CPD distributed radius becomes easier, when $-0.5 \leq \Phi \leq 0.5$. Therefore, we set $\Phi(r) = \int_{0}^{r} f(x)\,dx$, leading to

$$f(x) = \frac{D^2}{2\left(x^2 + D^2\right)^{3/2}}. \tag{12}$$

Setting $\Phi(r)$ equal to an evenly distributed random number $\xi \in [-0.5, 0.5]$ and inverting (12) allows us to obtain the SCD quantile function required for particle generation:

$$r = 2D\frac{\xi}{\sqrt{1 - 4\xi^2}}. \tag{13}$$

Therefore, in order to generate particles obeying the SCD distribution along the silicon wafer surface, each particle must be generated using (13), where ξ is an evenly distributed random number, $\xi \in [-0.5, 0.5]$.

B. Two-Dimensional SCD Distribution

When working with a three-dimensional model for AFM nanodots, a two-dimensional particle distribution is required. The analysis is similar to the one-dimensional model presented in the previous section. The derivation of the quantile function is performed using polar coordinates for simplicity and for easier generation of a final radial distribution of particles. For polar coordinates (r_n, θ) it is important to note that $x^2 + y^2 = r_n^2$, and $dxdy = r_n dr_n d\theta$. The two-dimensional PDF is

$$f(r_n, \theta) = -C\frac{DQ}{2\pi\left(r_n^2 + D^2\right)^{3/2}}. \tag{14}$$

The normalization constant C is found by the same procedure used for the one-dimensional model, to be $C = -1/Q$ and the normalized two-dimensional PDF becomes

$$f(r_n, \theta) = \frac{D}{2\pi\left(r_n^2 + D^2\right)^{3/2}}. \tag{15}$$

The cumulative probability distribution is then found by integrating the normalized PDF. The quantile function for the two-dimensional SCD distribution is then found by inverting the SCD function to obtain

$$r = D\sqrt{\frac{1}{(1-\xi)^2} - 1}, \tag{16}$$

where ξ is an evenly distributed random number, $\xi \in [0, 1]$. The normalized cross-section of a nanodot generated using this distribution is compared to the normalized SCD from (8) in Fig. 2.

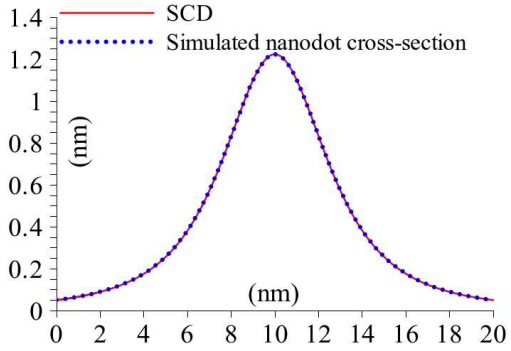

Fig. 2. Nanodot cross section compared with the SCD function.

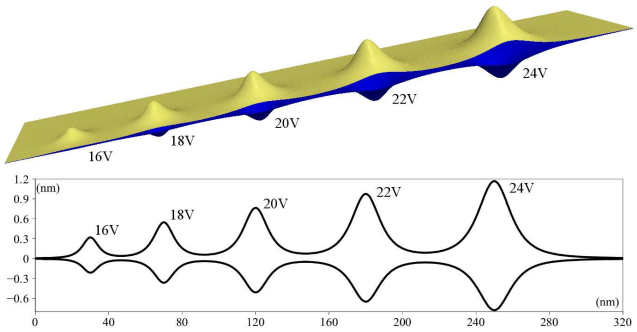

Fig. 3. The effect of voltage variation for AFM generated nanodot heights and widths.

IV. NC-AFM Nanodot and Nanowire Simulations

A. AFM Nanodot

The AFM nanodots shown in Fig. 3 were generated using the described model from [17] with added humidity effects and the two-dimensional SCD distribution explained in the previous sections. The nanodots show the modified topography of a silicon surface after AFM application with various bias voltages. The ambient humidity is set to 55% and the pulse time to 0.125ms. The top surface represents the interface between the AFM oxide nanodot and the ambient, while the bottom surface represents the interface between the AFM oxide nanodot and the silicon substrate.

B. AFM Nanowire as a Sequence of AFM Nanodots

In [17] it is suggested that a nanowire, which is patterned using a combination of AFM nanodots, separated at 0.5nm intervals will have an increased half-width due to the increased time for the lateral diffusion of anions. This phenomenon was added to the simulator and a nanodot was generated in the LS simulator to mimic the one presented in [17], as is shown in Fig. 4. As in [17], generating nanodots with 20V pulses for 1ms, while displacing the tip laterally by 0.5nm resulted in a nanowire with a height of approximately 1nm and a half-width of 13nm.

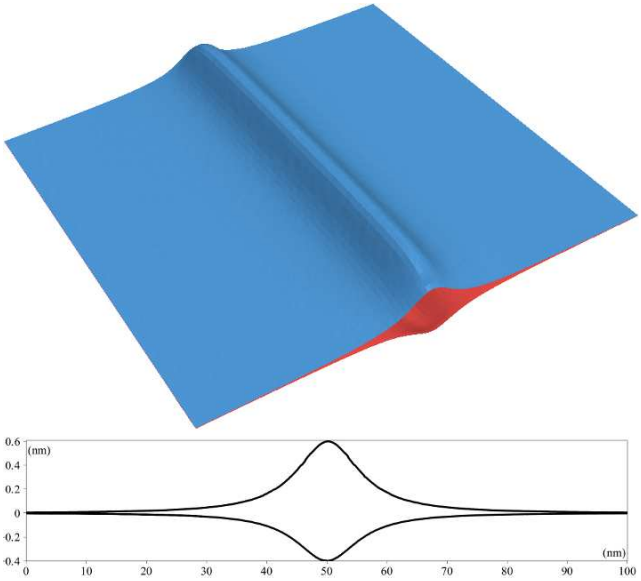

Fig. 4. Nanowire topography simulated using a sequence of AFM nanodots (top) and the nanowire's cross-section (bottom).

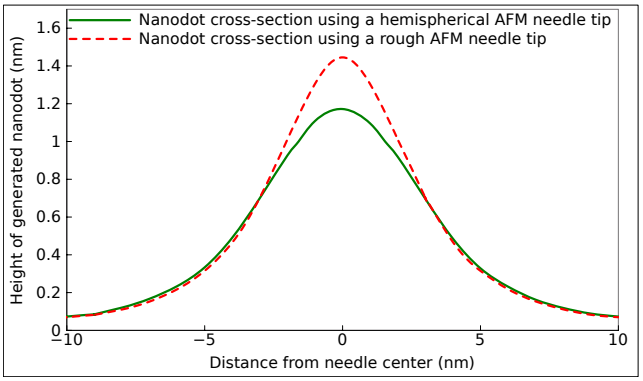

Fig. 5. Nanodot cross-sections generated using a hemispherical and a blunt AFM needle tip model. Blunt needle is modeled using a ring of 100 dot charges.

C. AFM Nanodot for Rough AFM Needle Tips

The SCD in (6) does not allow for a straight-forward derivation of a random distribution, such as the one shown in (13) and (16). Therefore, the Monte Carlo rejection technique is applied, whereby a test point is generated on the simulation domain using an even distribution, $\xi(x_t, y_t)$. An additional evenly distributed number between zero and σ_{max} is generated and, if this number is below $\sigma(x_t, y_t, 0)$, a particle is generated at (x_t, y_t, D). Otherwise, the location (x_t, y_t, D) is ignored and a new test point is generated. This procedure is repeated until a sufficient number of particles is kept in order to generate a nanodot topography. A comparison between nanodots generated using a hemispherical and rough needle tip is shown in Fig. 5. It is evident that a blunt needle tip will result in a blunt nanodot formation with a slight increase in lateral spreading.

V. Conclusion

Local oxidation nanolithography implemented with an AFM microscope has proven to be a useful tool for the generation of nanosized patterns on a silicon wafer surface. A model for the generation of nanodots and nanowires with non-contact AFM tools is presented. The AFM needle tip provides a voltage bias, which leads to the generation of a water meniscus between the needle and the sample surface. An electric field is generated within the water meniscus, causing the generation of oxyanions (OH-) and accelerating them towards the silicon, where an oxidation reaction is initiated. The tip is modeled by one or more charged dots in order to simulate the generated electric field and the resulting SCD distribution. The SCD function is derived for a one-dimensional and a two-dimensional SCD distribution, which makes the model useful for two-dimensional and three-dimensional AFM simulations, respectively.

References

[1] R. Garcia, R. V. Martinez, and J. Martinez, "Nano-chemistry and scanning probe nanolithographies," *Chem. Soc. Rev.*, vol. 35, pp. 29–38, 2006.

[2] S. Chou, P. Krauss, and P. Renstrom, "Imprint lithography with 25-nanometer resolution," *Science*, vol. 272, no. 5258, pp. 85–87, 1996.

[3] Y. Xia and G. Whitesides, "Soft lithography," *Angew. Chem. Int.*, vol. 37, pp. 550–575, 1998.

[4] J. Dagata et al., "Modification of hydrogen-passivated silicon by a scanning tunneling microscope operating in air," *Appl. Phys. Lett.*, vol. 56, pp. 2001–2003, 1990.

[5] G. Binning, H. Rohrer, C. Gerber, and E. Weibel, "Surface studies by scanning tunneling microscopy," *Phys. Rev. Lett.*, vol. 49, pp. 57–61, 1982.

[6] G. Binning, C. F. Quate, and C. Gerber, "Atomic force microscope," *Phys. Rev. Lett.*, vol. 56, pp. 930–933, 1986.

[7] Q. Tang, S. Shi, and L. Zhou, "Nanofabrication with atomic force microscopy," *J. Nanosci. Nanotechnol.*, vol. 4, pp. 948–963, 2004.

[8] R. V. Martinez et al., "Patterning polymeric structures with 2nm resolution at 3nm half pitch in ambient conditions," *Nano Lett.*, vol. 7, no. 7, pp. 1846–1850, 2007.

[9] G. Qin and C. Cai, "Sub-10-nm patterning of oligo (ethylene glycol) monolayers on silicon surfaces via local oxidation using a conductive atomic force microscope," *Nanotechnology*, vol. 20, no. 35, p. 355306, 2009.

[10] A. Notargiacomo and A. Tseng, "Assembling uniform oxide lines and layers by overlapping dots and lines using afm local oxidation," in *IEEE-NANO*, 2009, pp. 907–910.

[11] D. Stiévenard, P. Fontaine, and E. Dubois, "Nanooxidation using a scanning probe microscope: an analytical model based on field induced oxidation," *Appl. Phys. Lett.*, vol. 70, pp. 3272–3274, 1997.

[12] S. D. et al., "Effects of the electric field shape on nano-scale oxidation," *Surf. Sci.*, vol. 601, no. 23, pp. 5340–5358, 2007.

[13] A. Orians, C. Clemons, D. Golovaty, and G. Young, "One-dimensional dynamics of nano-scale oxidation," *Surf. Sci.*, vol. 600, no. 16, pp. 3297–3312, 2006.

[14] O. Ertl and S. Selberherr, "A fast Level Set framework for large three-dimensional topography simulations," *Computer Physics Communications*, vol. 180, no. 8, pp. 1242–1250, 2009.

[15] G. Mesa, E. DobadoFuentes, and J. J. Saenz, "Image charge method for electrostatic calculations in field-emission diodes," *J. Appl. Phys.*, vol. 79, no. 1, pp. 39–44, 1996.

[16] L. Filipovic and S. Siegfried, "A Monte Carlo simulator for non-contact mode atomic force microscopy," *LNCS/LSSC Proceedings*, vol. 7116, pp. 447–454, 2012.

[17] M. Calleja and R. García, "Nano-oxidation of silicon surfaces by noncontact atomic-force microscopy: size dependence on voltage and pulse duration," *Appl. Phys. Lett.*, vol. 76, no. 23, pp. 3427–3429, 2000.